### Controlling Frequency-Domain Hong-Ou-Mandel Interference via Electromagnetically Induced Transparency

Zi-Yu Liu<sup>1,2</sup>, Jiun-Shiuan Shiu<sup>1,2</sup>, Chin-Yao Cheng<sup>1,2</sup>, and Yong-Fan Chen<sup>1,2,3\*</sup>
<sup>1</sup>Department of Physics, National Cheng Kung University, Tainan 70101, Taiwan
<sup>2</sup>Center for Quantum Frontiers of Research & Technology, Tainan 70101, Taiwan
<sup>3</sup>Center for Quantum Technology, Hsinchu 30013, Taiwan

Hong–Ou–Mandel (HOM) interference is a compelling quantum phenomenon that demonstrates the nonclassical nature of single photons. Herein, we investigate an electromagnetically induced transparency-based double-Λ four-wave mixing system from the perspective of quantized light fields. The system can be used to realize efficient HOM interference in the frequency domain. By using the reduced density operator theory, we demonstrate that, although the double-Λ medium does not exhibit phase-dependent properties for the closed-loop case of two incident single photons, frequency-domain HOM two-photon interference occurs. For experimentally achievable optical depth conditions, our theory indicates that this double-Λ scheme can perform high-fidelity Hadamard gate operations on frequency-encoded single-photon qubits, and thereby generate HOM two-photon NOON states with a fidelity greater than 0.99. Furthermore, we demonstrate that this scheme can be used to realize arbitrary single-qubit gates and two-qubit SWAP gates by simply controlling the laser detuning and phase, exhibiting its multifunctional properties and providing a new route to scalable optical quantum computing.

#### I. INTRODUCTION

Hong-Ou-Mandel (HOM) interference [1-3], a wellknown quantum effect without a classical counterpart, has played a key role in optical quantum information processing [4–7] and quantum metrology [8–11]. Instead of passive devices, such as spatial or polarizing beam splitters, recent studies have used frequency converters to transfer HOM interference from the spatial to the spectral domain; this method facilitates quantum frequency multiplexing and engineering [12–15]. Studies of frequency-domain HOM interference for single photons have relied on linear optics, which involve the use of electro-optic phase modulators [16–18], or the nonlinear effects of solid materials [19-21]. Both schemes operate under far-detuned interaction conditions and thus require high-voltage amplifiers or strong pump light; however, these methods often generate adjacent sidebands or parametric noise photons, reducing the visibility of HOM interference [22, 23]. Herein, we propose another promising scheme based on near-resonant nonlinear optics that enables frequency-domain HOM interference with high visibility. The proposed scheme leverages the closed-loop four-wave mixing (FWM) effect in a double- $\Lambda$  electromagnetically induced transparency (EIT) system [24]. Because of the EIT effect, this near-resonant FWM scheme can substantially suppress vacuum field noise at low light levels, thereby effectively preventing photon dissipation and avoiding the generation of noise photons [25]. Such properties enable this double- $\Lambda$ scheme to generate frequency-domain HOM two-photon NOON states with extremely high fidelity.

To study frequency-domain HOM interference in a

closed-loop double- $\Lambda$  medium, we constructed a quantum model based on the reduced density operator theory [26]. Unlike semiclassical approaches, the proposed model quantizes two incident weak light fields. No discussion of such closed-loop FWM systems from the perspective of quantized light fields was found in a literature review. Previous semiclassical models have demonstrated that the respective transmittances of the two incident light fields through a closed-loop double- $\Lambda$  medium are affected by the relative phases of the applied light fields; this is known as the phase-dependent property [27–29]. However, our quantum model revealed that the phasedependent property of a closed-loop double- $\Lambda$  medium depends on the quantum states of the two incident weak light fields. If both incident weak light fields are in coherent states, the double- $\Lambda$  medium exhibits phasedependent properties, which is consistent with the predictions of a semiclassical model and has been experimentally confirmed [30–32]. By contrast, if both incident weak light fields are single photons, this phasedependent property is no longer present. Although the double- $\Lambda$  medium does not have phase-dependent properties in the case of two incident single photons, frequencydomain HOM interference of the two-photon state occurs. Our theory shows that such a double- $\Lambda$  scheme can perform high-fidelity Hadamard gate operations on frequency-encoded single-photon qubits. For experimentally achievable optical depth (OD) conditions, HOM two-photon NOON states with a fidelity of 0.99 can be generated. Furthermore, we demonstrate for the first time that this scheme can be used to implement arbitrary single-qubit gates and high-fidelity two-qubit SWAP gates, revealing its advantages in fabricating multifunctional photonic logic gates.

<sup>\*</sup> yfchen@ncku.edu.tw

#### II. THEORETICAL MODEL

We consider a medium comprising double- $\Lambda$  four-level atoms with two metastable ground states and two excited states [Fig. 1(a)]. The weak probe field  $\hat{a}_p$  driving the  $|1\rangle \leftrightarrow |3\rangle$  transition and the weak signal field  $\hat{a}_s$  driving the  $|1\rangle \leftrightarrow |4\rangle$  transition can both be described by quantum operators obeying the bosonic commutation relation. High-intensity coherent coupling and driving fields, described by the semiclassical Rabi frequency  $\Omega_{c(d)} = |\Omega_{c(d)}|e^{i\phi_{c(d)}}$  with a well-defined phase  $\phi_{c(d)}$ , drive  $|2\rangle \leftrightarrow |3\rangle$  and  $|2\rangle \leftrightarrow |4\rangle$  transitions, respectively, forming a closed-loop double-Λ EIT system together with the probe and signal fields. The parameters  $\gamma_{31}$  and  $\gamma_{41}$  represent the total coherence decay rates of the excited states  $|3\rangle$  and  $|4\rangle$ , respectively.  $\gamma_{21}$  is the dephasing rate between the ground states  $|1\rangle$  and  $|2\rangle$ . We consider the case in which the signal field and the driving field satisfy the two-photon resonance condition, but a one-photon detuning, denoted as  $\Delta$ , exists. By using the collective atomic operator approach and ignoring interactions between atoms, the interaction Hamiltonian  $\hat{H}$ of the double- $\Lambda$  system can be expressed as follows:

$$\hat{H} = -\frac{\hbar N}{2L} \int_0^L \left[ 2g_p \hat{\sigma}_{31}(z, t) \hat{a}_p(z, t) + 2g_s \hat{\sigma}_{41}(z, t) \hat{a}_s(z, t) + \Omega_c \hat{\sigma}_{32}(z, t) + \Omega_d \hat{\sigma}_{42}(z, t) + \Delta \hat{\sigma}_{44}(z, t) + \text{h.c.} \right] dz,$$
(1)

where N and L are the total number of atoms and the atomic medium length, respectively.  $g_p = \frac{d_{31}\varepsilon_p}{\hbar}$  denotes the coupling constant between the probe field and the single atom, where  $d_{31}$  is the dipole moment of the corresponding  $|3\rangle\leftrightarrow|1\rangle$  transition and  $\varepsilon_p=\sqrt{\frac{\hbar\omega_p}{2\epsilon_0 V}}$  is the electric field of the single probe photon. Similarly, there are  $g_s=\frac{d_{41}\varepsilon_s}{\hbar}$  and  $\varepsilon_s=\sqrt{\frac{\hbar\omega_s}{2\epsilon_0 V}}$  parameters for the signal field.  $\hat{\sigma}_{jk}(z,t)$  represents a collective atomic operator in the slowly-varying amplitude approximation [33] that obeys the following Heisenberg–Langevin equation (HLE) between states  $|j\rangle$  and  $|k\rangle$ 

$$\frac{\partial}{\partial t}\hat{\sigma}_{jk} = \frac{i}{\hbar}[\hat{H}, \hat{\sigma}_{jk}] - \frac{\gamma_{jk}}{2}\hat{\sigma}_{jk} + \gamma_{jk}^{sp} + \hat{F}_{jk}, \qquad (2)$$

where  $\gamma_{jk}^{sp}$  is the parameter related to the spontaneous decay process, and  $\hat{F}_{jk}$  denotes the associated Langevin noise operator. For the double- $\Lambda$  EIT system, both the probe and signal fields can be regarded as perturbation fields. Therefore, we can solve the first-order atomic operators by substituting the zero-order perturbation re-

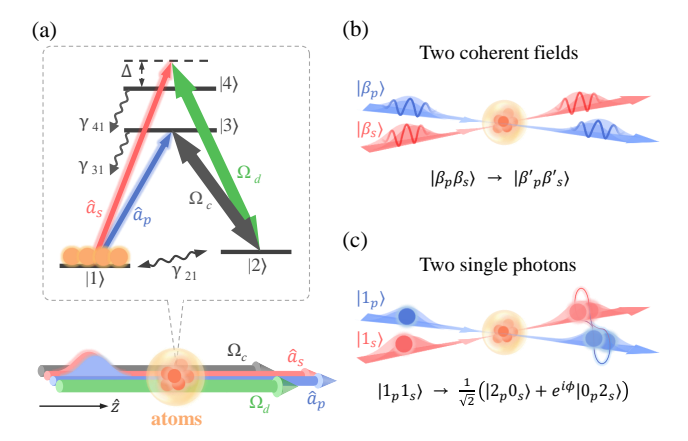


FIG. 1. Diagram of the four-level double-Λ EIT system. (a) The corresponding transitions for the four applied light fields. All light fields are assumed to propagate in the same direction to eliminate the Doppler shift in the atomic medium. (b) Both the input probe and signal fields are in coherent states. In this case, the two coherent fields  $|\beta_p\rangle$  and  $|\beta_s\rangle$  interfere in the double-Λ medium, and the output of the two coherent fields depends on the relative phase of the applied light fields. (c) Input probe and signal fields are two single photons (i.e.,  $|1_p 1_s\rangle$ ). In this case, although the phase-dependent property of the double-Λ medium is no longer present, HOM interference of the two-photon state occurs. The frequency-domain two-photon NOON state can be generated simply by optimizing the OD and  $\Delta$ .

sults into the relevant first-order HLEs as follows:

$$\frac{\partial}{\partial t}\hat{\sigma}_{21}^{(1)}(z,t) = \hat{F}_{21}(z,t) - \frac{1}{2}\gamma_{21}\hat{\sigma}_{21}^{(1)}(z,t) 
- i\left[\frac{\Omega_c}{2}\hat{\sigma}_{31}^{(1)}(z,t) + \frac{\Omega_d}{2}\hat{\sigma}_{41}^{(1)}(z,t)\right], \tag{3}$$

$$\frac{\partial}{\partial t}\hat{\sigma}_{31}^{(1)}(z,t) = \hat{F}_{31}(z,t) - \frac{1}{2}\gamma_{31}\hat{\sigma}_{31}^{(1)}(z,t) 
- i\left[g_p\hat{a}_p^{\dagger}(z,t) + \frac{\Omega_c^*}{2}\hat{\sigma}_{21}^{(1)}(z,t)\right], \tag{4}$$

$$\frac{\partial}{\partial t}\hat{\sigma}_{41}^{(1)}(z,t) = \hat{F}_{41}(z,t) - \frac{1}{2}\gamma_{41}\hat{\sigma}_{41}^{(1)}(z,t) 
- i\left[g_s\hat{a}_s^{\dagger}(z,t) + \frac{\Omega_d^*}{2}\hat{\sigma}_{21}^{(1)}(z,t) + \Delta\hat{\sigma}_{41}^{(1)}(z,t)\right]. \tag{5}$$

To investigate the behavior of the probe and signal fields propagating in the double- $\Lambda$  medium, the solutions of  $\hat{\sigma}_{31}^{(1)}(z,t)$  and  $\hat{\sigma}_{41}^{(1)}(z,t)$  from the first-order HLEs are incorporated into the following Maxwell–Schrödinger equations (MSEs):

$$\left(\frac{\partial}{\partial t} + c\frac{\partial}{\partial z}\right)\hat{a}_p^{\dagger}(z,t) = -ig_p N\hat{\sigma}_{31}^{(1)}(z,t), \tag{6}$$

$$\left(\frac{\partial}{\partial t} + c\frac{\partial}{\partial z}\right)\hat{a}_s^{\dagger}(z,t) = -ig_s N\hat{\sigma}_{41}^{(1)}(z,t), \tag{7}$$

where c is the speed of light. Subsequently, through the Fourier transform from the time domain to the frequency

domain, the coupled equations of  $\tilde{a}_p^\dagger(z,\omega)$  and  $\tilde{a}_s^\dagger(z,\omega)$  can be derived as follows:

$$\frac{\partial}{\partial z}\tilde{a}_{p}^{\dagger} + \Lambda_{p}\tilde{a}_{p}^{\dagger} + \kappa_{p}e^{i(-\phi_{c} + \phi_{d})}\tilde{a}_{s}^{\dagger} = \sum_{jk} \zeta_{jk}^{p}\tilde{f}_{jk}, \qquad (8)$$

$$\frac{\partial}{\partial z}\tilde{a}_s^{\dagger} + \Lambda_s \tilde{a}_s^{\dagger} + \kappa_s e^{-i(-\phi_c + \phi_d)} \tilde{a}_p^{\dagger} = \sum_{jk} \zeta_{jk}^s \tilde{f}_{jk}, \qquad (9)$$

where  $\Lambda_{p(s)}$  and  $\kappa_{p(s)}$  are the EIT dispersion coefficient and coupling constant of the probe (signal) transition, respectively [34].  $\tilde{f}_{jk} \equiv \sqrt{\frac{N}{c}} \tilde{F}_{jk}$  is the renormalized Langevin noise operator, where  $jk \in \{21,31,41\}$  denotes the subscript of the atomic operator  $\tilde{\sigma}_{jk}$ .  $\zeta_{jk}^p$  and  $\zeta_{jk}^s$  are the coefficients of the Langevin noise operators of interest. For simplicity, we consider the steady-state case of  $\omega=0$  and assume that  $|\Omega_c|=|\Omega_d|\equiv |\Omega|,\ g_p=g_s\equiv g,\ \gamma_{31}=\gamma_{41}\equiv \Gamma,$  and  $\gamma_{21}=0.$  Under these conditions, the general solution of the aforementioned coupled equations can be obtained as follows:

$$\begin{bmatrix} \tilde{a}_{p,L}^{\dagger} \\ \tilde{a}_{s,L}^{\dagger} \end{bmatrix} = e^{-ML} \begin{bmatrix} \tilde{a}_{p,0}^{\dagger} \\ \tilde{a}_{s,0}^{\dagger} \end{bmatrix} + \sum_{jk} \int_{0}^{L} e^{-M(L-z)} \begin{bmatrix} \zeta_{jk}^{p} \\ \zeta_{jk}^{s} \end{bmatrix} \tilde{f}_{jk} dz, \tag{10}$$

where  $\tilde{a}_{p(s),L}^{\dagger}$  and  $\tilde{a}_{p(s),0}^{\dagger}$  are abbreviations for  $\tilde{a}_{p(s)}^{\dagger}(L,0)$  and  $\tilde{a}_{p(s)}^{\dagger}(0,0)$ , respectively. All the coefficients of the general solution can be found in Appendix A. The term  $e^{-ML}$  characterizes the parametric evolution of the double- $\Lambda$  medium. Its matrix form is

$$e^{-ML} = \exp\left(-\begin{bmatrix} \Lambda_p & \kappa_p e^{i(-\phi_c + \phi_d)} \\ \kappa_s e^{-i(-\phi_c + \phi_d)} & \Lambda_s \end{bmatrix} L\right)$$

$$\equiv \begin{bmatrix} A & B \\ C & D \end{bmatrix}. \tag{11}$$

The second term on the right-hand side of Eq. (10) describes the quantum fluctuation effect induced by the vacuum field reservoir. To enable correspondence with more commonly used parameters, we use the substitution  $\frac{\alpha\Gamma}{4L}=\frac{g^2N}{c}$ , where  $\alpha$  denotes the OD of the atomic medium. Therefore, the matrix elements in Eq. (11) are obtained as

$$A = \frac{1}{2} \left[ 1 + e^{i\alpha\Gamma/2(\Delta - i\Gamma)} \right], \tag{12}$$

$$B = \frac{1}{2} \left[ 1 - e^{i\alpha\Gamma/2(\Delta - i\Gamma)} \right] e^{-i(\phi_c - \phi_d)}, \quad (13)$$

$$C = \frac{1}{2} \left[ 1 - e^{i\alpha\Gamma/2(\Delta - i\Gamma)} \right] e^{i(\phi_c - \phi_d)}, \tag{14}$$

$$D = \frac{1}{2} \left[ 1 + e^{i\alpha\Gamma/2(\Delta - i\Gamma)} \right]. \tag{15}$$

In Eq. (10), A and C (D and B) represent the mode-preserved and mode-converted coefficients, respectively, of the probe (signal) field propagating in the double- $\Lambda$  medium. These coefficients are similar to the transmission and reflection coefficients of light passing through a spatial beam splitter.

To investigate the response of the double- $\Lambda$  medium to different input photon quantum states, the density matrix of the output state,  $\rho_f = \tilde{U} \rho_i \tilde{U}^\dagger$ , is constructed in accordance with the density matrix of the input state  $\rho_i$  and the evolution operator  $\tilde{U}$  of the combined system in the frequency domain, where  $\rho_i = \rho^{PS}(z=0,\omega) \otimes \rho^R$  is in the product form of the incident probe and signal fields  $\rho^{PS}$  and the reservoir  $\rho^R$ . In accordance with the reduced density operator approach in Ref. [35] and under the steady-state condition, the matrix element of the output probe and signal fields in the Fock-state basis is given by

$$\rho_{m_{p}m_{s}n_{p}n_{s}}^{PS}(L,0) = \text{Tr}\left\{\tilde{\rho}_{m_{p}m_{s}n_{p}n_{s}}(L,0)\rho_{i}\right\},$$
 (16)

where  $\tilde{\rho}_{m_p m_s n_p n_s}(L,0) = \tilde{U}^{\dagger} (|n_p n_s\rangle \langle m_p m_s| \otimes I_R) \tilde{U}$  is the operator for the matrix element of the output probe and signal fields. If Eq. (10) is applied and the vacuum density matrix with annihilation and creation operators are rewritten as  $|0\rangle\langle 0| = \sum_{l=0}^{\infty} \frac{(-1)^l}{l!} (\tilde{a}^{\dagger})^l (\tilde{a})^l$ , the operator  $\tilde{\rho}_{m_p m_s n_p n_s}$  can be derived as

$$\tilde{\rho}_{m_{p}m_{s}n_{p}n_{s}}(L,0) 
= \sum_{l_{p},l_{s}=0}^{\infty} \chi_{mnl} (A\tilde{a}_{p,0}^{\dagger} + B\tilde{a}_{s,0}^{\dagger})^{l_{p}+n_{p}} (C\tilde{a}_{p,0}^{\dagger} + D\tilde{a}_{s,0}^{\dagger})^{l_{s}+n_{s}} 
\times (A^{*}\tilde{a}_{p,0} + B^{*}\tilde{a}_{s,0})^{l_{p}+m_{p}} (C^{*}\tilde{a}_{p,0} + D^{*}\tilde{a}_{s,0})^{l_{s}+m_{s}},$$
(17)

where  $\chi_{mnl} = \frac{1}{\sqrt{m_p!m_s!n_p!n_s!}} \frac{(-1)^{l_p+l_s}}{l_p!l_s!}$ . In the derivation of Eq. (17), the normal-ordered noise caused by the Langevin operator  $\tilde{f}_{jk}$  is proportional to the atomic population of the excited state [36]; hence, it can be ignored under the perturbation condition of the weak probe and signal fields (see Appendix B for more details).

#### III. TWO COHERENT FIELDS

We first consider the case of two coherent fields passing through the double- $\Lambda$  medium. As indicated in Fig. 1(b), the two coherent states with probe and signal frequency modes, respectively, are the initial states  $|\psi_i^{PS}\rangle = |\beta_p\rangle \otimes |\beta_s\rangle$ . If Eqs. (16) and (17) are calculated, the matrix element of the the output probe and signal fields can be obtained as

$$\rho_{m_{p}m_{s}n_{p}n_{s}}^{PS}(L,0) = \sum_{l_{p},l_{s}=0}^{\infty} \chi_{mnl} (A\beta_{p}^{*} + B\beta_{s}^{*})^{l_{p}+n_{p}} (C\beta_{p}^{*} + D\beta_{s}^{*})^{l_{s}+n_{s}} \times (A^{*}\beta_{p} + B^{*}\beta_{s})^{l_{p}+m_{p}} (C^{*}\beta_{p} + D^{*}\beta_{s})^{l_{s}+m_{s}} \\
= e^{-|A^{*}\beta_{p} + B^{*}\beta_{s}|^{2}} \frac{(A^{*}\beta_{p} + B^{*}\beta_{s})^{m_{p}} (A\beta_{p}^{*} + B\beta_{s}^{*})^{n_{p}}}{\sqrt{m_{p}!n_{p}!}} \times e^{-|C^{*}\beta_{p} + D^{*}\beta_{s}|^{2}} \frac{(C^{*}\beta_{p} + D^{*}\beta_{s})^{m_{s}} (C\beta_{p}^{*} + D\beta_{s}^{*})^{n_{s}}}{\sqrt{m_{s}!n_{s}!}}, \tag{18}$$

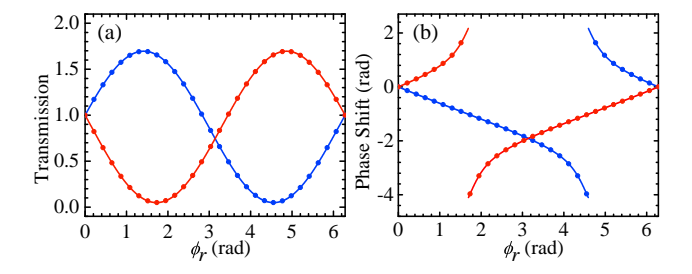


FIG. 2. The closed-loop case of two incident weak coherent fields. (a) Transmission and (b) phase shift of the probe (blue) and signal (red) coherent fields versus  $\phi_r$  plotted using the quantum (solid) and semiclassical (dotted) models under conditions of  $|\beta_p| = |\beta_s|$ ,  $\Delta = 13\Gamma$ , and OD = 50.

by which the output state of the probe and signal fields becomes

$$|\psi_f^{PS}\rangle = |A^*\beta_p + B^*\beta_s\rangle \otimes |C^*\beta_p + D^*\beta_s\rangle$$
  

$$\equiv |\beta_p'\rangle \otimes |\beta_s'\rangle, \tag{19}$$

where both the output probe  $|\beta_p'\rangle$  and signal  $|\beta_s'\rangle$  fields remain in coherent states, indicating that the double- $\Lambda$  medium only coherently redistributes the incident probe and signal amplitudes through the EIT-based FWM process without changing the photon statistics of these two coherent fields or entangling them [37]. Furthermore, Eq. (19) reveals that the amplitude and phase changes of the output probe and signal fields depend on the relative phase of the applied light fields. The transmittances and phase shifts of the probe and signal fields through the double- $\Lambda$  medium are given by

$$T_p = \left| \frac{\beta_p'}{\beta_p} \right|^2 = \left| A^* + u_\beta B'^* e^{-i\phi_r} \right|^2,$$
 (20)

$$\Delta \phi_p = \arg \left[ \frac{\beta_p'}{\beta_p} \right] = \arg \left[ A^* + u_\beta B'^* e^{-i\phi_r} \right], \qquad (21)$$

$$T_s = \left| \frac{\beta_s'}{\beta_s} \right|^2 = \left| u_\beta^{-1} C'^* e^{i\phi_r} + D^* \right|^2, \tag{22}$$

$$\Delta \phi_s = \arg \left[ \frac{\beta_s'}{\beta_s} \right] = \arg \left[ u_\beta^{-1} C'^* e^{i\phi_r} + D^* \right], \qquad (23)$$

where  $B'^* \equiv B^* e^{-i(\phi_c - \phi_d)}$ ,  $C'^* \equiv C^* e^{i(\phi_c - \phi_d)}$ ,  $u_\beta \equiv |\beta_s|/|\beta_p|$  is the ratio of the probe and signal amplitudes, and  $\phi_r \equiv (\phi_p - \phi_s) - (\phi_c - \phi_d)$  is the relative phase of the applied light fields. Figure 2 reveals that the theoretical curves of transmittance and phase shift, as a function of the relative phase  $\phi_r$  for the probe and signal fields obtained from the current quantum model (solid lines), are identical to those of the semiclassical model (dotted lines) in Ref. [30]. If the input light fields are all in coherent states, this closed-loop double- $\Lambda$  medium exhibits phase-dependent properties, which have been experimentally investigated in atomic ensembles [30–32].

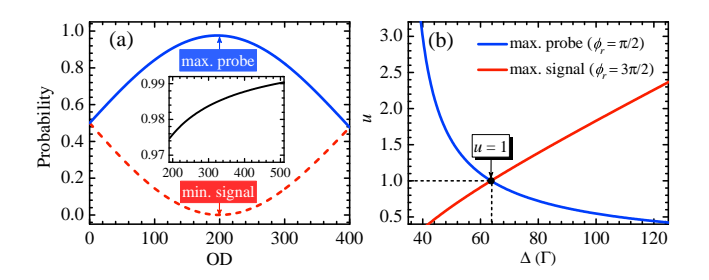


FIG. 3. Hadamard gates for single-photon two-color qubits. (a) Probability that the two-color qubit with u=1 and  $\phi_u=0$  is in the probe frequency mode  $(P_{1p0s},$  solid blue) and the signal frequency mode  $(P_{0p1s},$  dashed red) versus OD under the conditions of  $\phi_r=\pi/2$  and  $\Delta=(200/\pi)\Gamma$ . Inset: For  $\Delta=(\mathrm{OD}/\pi)\Gamma$ , the maximum probability approaches 1 as OD increases. (b) Theoretical  $\Delta$  curves for maximizing the probabilities of  $|1_p0_s\rangle$  (solid blue) and  $|0_p1_s\rangle$  (solid red) as a function of u for  $\mathrm{OD}=200$ . The two curves intersect at u=1 where  $\Delta=(200/\pi)\Gamma$ , which is the condition in (a).

#### IV. HADAMARD GATES

We next consider a single-photon qubit case in which an incident single photon has entangled probe and signal frequency modes, namely

$$|\psi_i^{PS}\rangle = \frac{1}{\sqrt{1+u^2}} \left( |1_p 0_s\rangle + u e^{-i\phi_u} |0_p 1_s\rangle \right), \quad (24)$$

where u is a parameter indicating the amplitude ratio between the probe and signal frequency modes, and  $\phi_u$  denotes the relative phase between the two modes. A single photon with a superposition state of two frequency modes is also called a frequency-encoded photonic qubit or two-color qubit [38]. Here,  $\phi_u$  is similar to the role of the relative phase  $(\phi_p - \phi_s)$  between the two coherent fields mentioned in the previous section. Therefore, in the case of a single-photon two-color qubit, the double- $\Lambda$  medium can also be expected to exhibit phase-dependent properties. To confirm this, the probability that the output single photon is in the probe and signal frequency modes, respectively, can be determined using Eqs. (16) and (17) as follows:

$$P_{1p0s} = \rho_{1010}^{PS} = \frac{1}{1+u^2} \left| A^* + uB'^* e^{-i\phi_r} \right|^2, \qquad (25)$$

$$P_{0p1s} = \rho_{0101}^{PS} = \frac{1}{1+u^2} \left| C^{\prime *} e^{i\phi_r} + uD^* \right|^2, \qquad (26)$$

where  $\phi_r = \phi_u - (\phi_c - \phi_d)$  is equivalent to the relative phase in the previous case of two coherent fields with  $\phi_u = \phi_p - \phi_s$ . As expected, these results verify the dependence of the output state of the single-photon qubit on the relative phase of the applied light fields in the double- $\Lambda$  medium. Figure 3(a) plots the theoretical curves of  $P_{1p0s}$  and  $P_{0p1s}$  as a function of OD under the conditions of  $\phi_r = \pi/2$  and  $\Delta = (200/\pi) \Gamma$  for single-photon qubits with equal-amplitude and in-phase modes, namely u=1 and  $\phi_u=0$ . The theoretical curves reveal that  $P_{1p0s}$ 

increases as OD increases and reaches a maximum value close to 1 at OD = 200, whereas  $P_{0p1s}$  decreases to almost zero. In other words, under these conditions, the two-color single photon entering the double- $\Lambda$  medium is converted into a single photon carrying only one color, which is equivalent to the Hadamard gate, and its operation fidelity can reach 0.99 at OD = 200.

The physics of this frequency-domain Hadamard gate can be described as follows. Because of the large detuning condition of  $\Delta = (OD/\pi)\Gamma$ , the amplitudes of the mode-preserved coefficient and mode-converted coefficient of the double- $\Lambda$  medium are almost equal; that is,  $|A| \approx |C| \approx 0.5 \text{ and } |D| \approx |B| \approx 0.5 \text{ [Eqs. (12)-(15)]}.$ In this case, when  $\phi_r = \pi/2$ , the probe mode-preserved coefficient  $A^*$  and the signal mode-converted coefficient  $B^{\prime*}e^{-i\pi/2}$  in Eq. (25) are almost in phase, resulting in constructive interference, which causes the output photon to be converted into the probe frequency mode (i.e.,  $P_{1,0,0}\approx 1$ ). However, if  $\phi_r$  is  $3\pi/2$ , the two aforementioned coefficients have out-of-phase destructive interference, causing the theoretical curves in Fig. 3(a) to become interchanged, and the output photon is converted to the signal frequency mode, resulting in  $P_{0_p 1_s} \approx 1$ .

For the input single-photon qubits with arbitrary uvalues, the output of  $|1_n0_s\rangle$  can be achieved by using a specific detuning value  $\Delta$  that satisfies the  $|A^*| = |uB'^*|$ condition. In this case, constructive interference in the probe frequency mode occurs if  $\phi_r = \pi/2$ . By contrast, the output of  $|0_p 1_s\rangle$  can be achieved by simply setting the relative phase  $\phi_r$  to  $3\pi/2$  and adjusting  $\Delta$  to satisfy the condition  $|C'^*| = |uD^*|$ . This suggests that the double- $\Lambda$  scheme can be used as a single-qubit gate with x-rotation and y-rotation. Therefore, arbitrary singlequbit gates can be realized by concatenating the x- and y-rotation gates based on this scheme [39]. Figure 3(b) presents plots of two theoretical curves of  $\Delta$  as a function of u required to achieve the maximum probabilities of  $|1_p 0_s\rangle$  and  $|0_p 1_s\rangle$  for OD = 200. The two curves intersect at u=1 and  $\Delta=(200/\pi)\Gamma$ , corresponding to the condition OD = 200 of Fig. 3(a). For one-color input single photons (u=0), the double- $\Lambda$  medium does not have phase-dependent properties because no interference occurs [Eqs. (25) and (26)]. This system is also known as an open-loop FWM system and can be used as an efficient frequency converter [40–44].

#### V. HOM INTERFERENCE

We now consider the case in which the two input single photons carry the probe and signal frequency modes, respectively. This is a two-photon state with no correlation between the modes, as depicted by  $|1_p\rangle\otimes|1_s\rangle$  in Fig. 1(c). As previously stated, under the ideal conditions of an extremely large OD value, the double- $\Lambda$  medium causes little photon dissipation. Therefore, the output photons only have the following three possible quantum states with corresponding probabilities: (1) state  $|2_p0_s\rangle$ , both

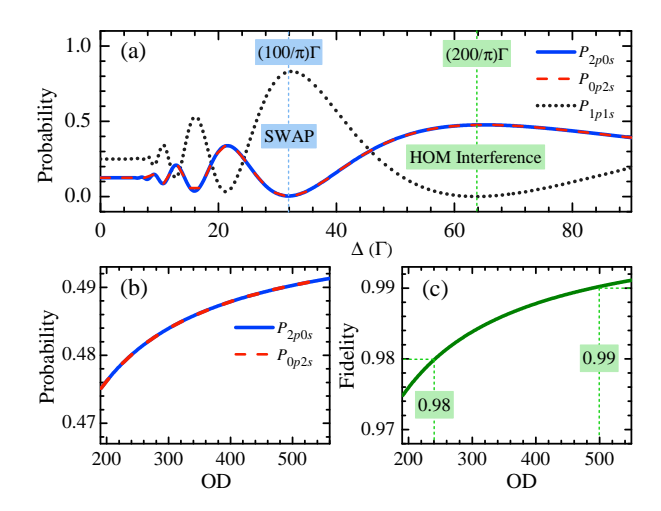


FIG. 4. HOM interference and color swap for two input single photons. (a) Theoretical curves for the probabilities  $P_{2p0s}$  (solid blue),  $P_{0p2s}$  (dashed red), and  $P_{1p1s}$  (dotted black) versus  $\Delta$  at OD = 200. HOM interference and two-photon swap occur at  $\Delta = (200/\pi)\Gamma$  and  $\Delta = (100/\pi)\Gamma$ , respectively. (b) At  $\Delta = (\text{OD}/\pi)\Gamma$ , the maximum probabilities of  $P_{2p0s}$  and  $P_{0p2s}$  tend to approach 1 as OD increases. (c) The fidelity of the HOM two-photon NOON state versus OD.

photons exit under the probe frequency mode with  $P_{2p0s}$ ; (2) state  $|0_p2_s\rangle$ , both photons exit under the signal frequency mode with  $P_{0p2s}$ ; (3) state  $|1_p1_s\rangle$ , photons exit with disparate colors with  $P_{1p1s}$ . These three probabilities are obtained as

$$P_{2p0s} = \rho_{2020}^{PS} = 2 |A^*B^*|^2, \qquad (27)$$

$$P_{0p2s} = \rho_{0202}^{PS} = 2 \left| C^* D^* \right|^2, \tag{28}$$

$$P_{1p1s} = \rho_{1111}^{PS} = |A^*D^* + B^*C^*|^2.$$
 (29)

Unlike the previous case of the input two-color qubit, the probabilities of the output states in this case are not affected by the relative phase of the applied light fields; they are phase-independent. This phenomenon is ascribed to the quantum uncertainty of the relative phase between the two input single photons, which prevents them from interfering with each other in the double- $\Lambda$  medium. However, quantum interference of the two-photon state occurs [Eqs. (27)–(29)].

Figure 4(a) presents plots of the probabilities  $P_{2p0s}$ ,  $P_{0p2s}$ , and  $P_{1p1s}$  versus  $\Delta$  at OD = 200. These theoretical curves reveal that if  $\Delta = (200/\pi)\Gamma$ , both  $P_{2p0s}$  and  $P_{0p2s}$  are close to 0.5, whereas  $P_{1p1s}$  approaches 0. That is, the input two-photon state  $|1_p1_s\rangle$  is almost completely suppressed by the double- $\Lambda$  medium, and the two single photons tend to have the same color, exhibiting HOM interference in the frequency domain. This phenomenon of two-photon state interference is caused by the operation of the Hadamard gate. If  $\Delta = (\text{OD}/\pi)\Gamma$ , the magnitudes of the coefficients for mode preservation and mode conversion are almost equal (approximately 0.5), which is the Hadamard gate operation and causes

the transition amplitudes  $A^*D^*$  (describing the two photons preserved in their respective modes) and  $B^*C^*$  (indicating that the modes of the two photons mutually swap) to have the same magnitude but be out of phase (i.e.,  $A^*D^* \approx -B^*C^*$ ). Therefore, destructive interference between the two transition amplitudes in Eq. (29) occurs, resulting in  $P_{1p1s} \approx 0$ .

When the laser is detuned as  $(100/\pi)\Gamma$  in Fig. 4(a), the two single photons exit with disparate colors; the state is  $|1_p1_s\rangle$ . In contrast with the two-photon HOM interference produced in the Hadamard gate operation, the mode-converted coefficients  $B^*$  and  $C^*$  are both approximately 1 in this case, whereas the mode-preserved coefficients  $A^*$  and  $D^*$  approach 0, resulting in  $P_{1p1s} \approx 1$  and  $P_{2p0s} \approx P_{0p2s} \approx 0$ . Thus, the two single photons mutually swap colors in a near-perfect frequency conversion process and end up in the same state  $|1_p1_s\rangle$ , which also shows that whether the output photons generate HOM interference or swap colors can be controlled in this double- $\Lambda$  scheme by simply adjusting the laser detuning conditions.

Figure 4(b) plots the theoretical curves of  $P_{2p0s}$  and  $P_{0p2s}$  versus OD under the HOM interference condition of  $\Delta = (\text{OD}/\pi) \Gamma$ . The theoretical results indicate that increasing OD can suppress the loss of output photons due to spontaneous emission. Therefore, if the OD value is large, the loss of output photons can be neglected, and its quantum state is obtained as

$$|\psi_f^{PS}\rangle = \frac{1}{\sqrt{2}} \left[ |2_p 0_s\rangle + e^{-2i(\phi_c - \phi_d)} |0_p 2_s\rangle \right],$$
 (30)

which is a two-photon NOON state in the frequency domain that has practical applications in photonic quantum metrology for its ability to conduct precision phase measurements if used in optical interferometers [45]. Although the amplitude of the two-photon NOON state is independent of the phases of the applied light fields, the relative phase between modes  $|2_p 0_s\rangle$  and  $|0_p 2_s\rangle$  can be controlled by varying  $\phi_c$  and  $\phi_d$ . Furthermore, for actual cases of finite OD, the two input single photons in the double- $\Lambda$  medium will be slightly dissipated, which not only causes the output photons to become a mixed state but also reduces the fidelity of the two-photon NOON state, as displayed in Fig. 4(c). The theoretical curve reveals that the fidelity approaches 1 as the OD increases owing to the proportional suppression of photon loss due to spontaneous emission in the double- $\Lambda$  EIT medium. If OD = 500, the fidelity can reach 0.99, which is a condition that can currently be achieved experimentally [46–48]. Hence, HOM interference based on the double- $\Lambda$  scheme is applicable for generating high-purity two-photon NOON states in the frequency domain.

#### VI. SWAP GATES

In the previous section, we have shown that when the condition  $\Delta = (OD/2\pi)\Gamma$  is satisfied, the colors of

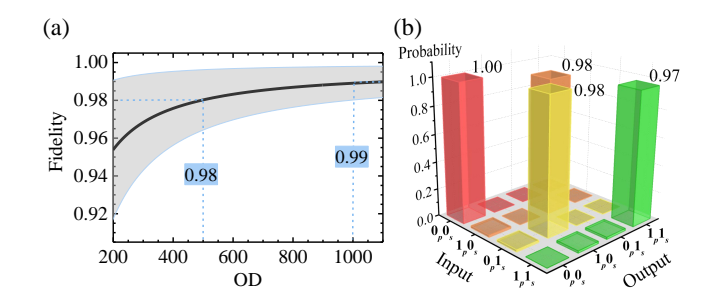


FIG. 5. Performance of the color SWAP gate. (a) Average (solid line) and standard deviation (gray area) of the SWAP gate fidelity plotted against the OD obtained from the density matrices of the output results according to the four computational input states. The vertical dash lines denote the OD of around 500 and 1000 for fidelities reaching 0.98 and 0.99, respectively. (b) Truth table of the SWAP process according to the output probabilities using the four inputs when  $\mathrm{OD}=1000$  in (a). Under this condition, the average success rate per gate operation is around 0.98.

two input single photons are exchanged in the double- $\Lambda$ medium [see Fig. 4(a)]. Next, we demonstrate that this double- $\Lambda$  scheme can be used as a high-fidelity two-qubit SWAP gate under this condition, which is essential for scalable quantum networks [49, 50]. Figure 5(a) presents the average (curve) and standard deviation (gray area) of the SWAP gate fidelity according to the four computational input states (i.e.,  $|0_p 0_s\rangle$ ,  $|1_p 0_s\rangle$ ,  $|0_p 1_s\rangle$ , and  $|1_p 1_s\rangle$ ) versus OD. The theoretical curve shows that the average fidelity approaches 1 as the OD increases. By contrast, the standard deviation of fidelity decreases with increasing OD. When OD = 500, the fidelity of the SWAP gate can reach 0.98. For the region of OD exceeding 1000, the SWAP gate achieves a high fidelity of F = 0.99 with a low standard deviation of 0.01. The truth table of the SWAP process when OD = 1000 is shown in Fig. 5(b). Under this condition, the average success probability per gate operation reaches 0.98, corresponding to an error rate of 0.02 for a single SWAP operation.

#### VII. CONCLUSION

We propose an EIT-based double- $\Lambda$  FWM system for achieving efficient HOM interference in the frequency domain. By considering quantized light fields, we theoretically elucidated the quantum properties of the double- $\Lambda$  medium. Our quantum model confirms that if the incident light fields are coherent states, the double- $\Lambda$  medium under closed-loop conditions has phase-dependent properties caused by the mutual interference of the light fields, consistent with the predictions of the semiclassical model. However, in the closed-loop case of two incident single photons, the double- $\Lambda$  medium no longer has this phase-dependence; instead, frequency-domain HOM interference of the two-photon state occurs. If laser detuning is controlled, the proposed double- $\Lambda$  scheme

can perform high-fidelity Hadamard gate operations on frequency-encoded single-photon qubits, and the scheme can generate HOM two-photon NOON states with a fidelity greater than 0.99 at OD = 500. This near-resonant FWM scheme based on double- $\Lambda$  EIT is a novel and promising scheme for frequency-domain HOM interference with high visibility, which has practical applications in photonic quantum metrology. In addition, we demonstrated that the proposed scheme can be used to realize arbitrary high-fidelity single-qubit gates and two-qubit SWAP gates by simply controlling the laser detuning and phase. These double- $\Lambda$  FWM-based photonic gates can be easily integrated with various EIT-related quantum technologies, such as quantum memories [51–56] and quantum repeaters [57–63], facilitating the development of quantum networks and scalable quantum information processing [64–68].

#### ACKNOWLEDGMENTS

The authors acknowledge Ite A. Yu, Ying-Cheng Chen, and Che-Ming Li for helpful discussions. This work was supported by the National Science and Technology Council of Taiwan under Grant No. 111-2112-M-006-027, No. 111-2639-M-007-001-ASP, and No. 111-2119-M-007-007.

# APPENDIX A: COEFFICIENTS OF COUPLED EQUATIONS

In Sec. II, we derive the frequency-domain coupled equations between the probe field and the signal field, as shown in Eqs. (8) and (9). All coefficients in Eq. (10) can be obtained as follows:

$$\Lambda_p = \Lambda_s = \frac{\alpha \Gamma}{4L} \left( \frac{1}{\Gamma + i\Delta} \right), \tag{A1}$$

$$\kappa_p = \kappa_s = -\frac{\alpha\Gamma}{4L} \left( \frac{1}{\Gamma + i\Delta} \right),$$
(A2)

$$\zeta_{21}^{p} = i\sqrt{\frac{\alpha\Gamma}{4L}} \left[ \frac{i\Gamma - 2\Delta}{(\Gamma + i\Delta)|\Omega|} \right] e^{-i\phi_c}, \tag{A3}$$

$$\zeta_{31}^p = -i\sqrt{\frac{\alpha\Gamma}{4L}} \left(\frac{1}{\Gamma + i\Delta}\right),\tag{A4}$$

$$\zeta_{41}^{p} = i\sqrt{\frac{\alpha\Gamma}{4L}} \left(\frac{1}{\Gamma + i\Delta}\right) e^{-i(\phi_c - \phi_d)}, \quad (A5)$$

$$\zeta_{21}^{s} = i\sqrt{\frac{\alpha\Gamma}{4L}} \left[ \frac{i\Gamma}{(\Gamma + i\Lambda)|\Omega|} \right] e^{-i\phi_d}, \tag{A6}$$

$$\zeta_{31}^{s} = i\sqrt{\frac{\alpha\Gamma}{4L}} \left(\frac{1}{\Gamma + i\Delta}\right) e^{i(\phi_c - \phi_d)}, \tag{A7}$$

$$\zeta_{41}^{s} = -i\sqrt{\frac{\alpha\Gamma}{4L}} \left(\frac{1}{\Gamma + i\Delta}\right). \tag{A8}$$

### APPENDIX B: NOISE CORRELATIONS AND DIFFUSION COEFFICIENTS

In the derivation of Eq. (17), we assume that the Langevin noise operator satisfies the delta correlation as follows:

$$\langle \tilde{f}_{jk}(z,\omega)\tilde{f}_{k'j'}(z',\omega')\rangle = \frac{L}{2\pi c}D_{jk,k'j'}\delta(z-z')\delta(\omega-\omega'),$$
(B1)

where  $D_{jk,k'j'}$  is the diffusion coefficient, which can be obtained using the Einstein relation [69] as follows:

$$D_{jk,k'j'} = \frac{\partial}{\partial t} \langle \hat{\sigma}_{jk} \hat{\sigma}_{k'j'} \rangle - \left\langle \left( \frac{\partial}{\partial t} \hat{\sigma}_{jk} - \hat{F}_{jk} \right) \hat{\sigma}_{k'j'} \right\rangle - \left\langle \hat{\sigma}_{jk} \left( \frac{\partial}{\partial t} \hat{\sigma}_{k'j'} - \hat{F}_{k'j'} \right) \right\rangle.$$
(B2)

For the case of  $\gamma_{21} = 0$  considered in the main text, we can obtain the diffusion coefficient of the double- $\Lambda$  atomic system through Eq. (B2). Its matrix form is

Under the condition of the weak probe and signal fields,  $\langle \hat{\sigma}_{33} \rangle \approx \langle \hat{\sigma}_{44} \rangle \approx 0$ , that is, all the normal-ordered noise correlations  $\langle \tilde{f}_{jk} \tilde{f}_{k'j'} \rangle$  are close to zero. According to Eq. (10), the normal-ordered noise correlations contribute additional photons to the probe and signal fields, i.e.  $\langle \tilde{a}_{p,L}^{\dagger} \tilde{a}_{p,L} \rangle$  and  $\langle \tilde{a}_{s,L}^{\dagger} \tilde{a}_{s,L} \rangle$ , which can be regarded as the spontaneous-emitted noise photons induced by the vacuum field reservoir. Additionally, we calculate the anti-normal-ordered noise terms,  $\langle \tilde{f}_{k'j'} \tilde{f}_{jk} \rangle$ . Under the same conditions, the corresponding diffusion coefficient matrix is

$$D_{k'j',jk} = \begin{bmatrix} D_{1221} & D_{1231} & D_{1241} \\ D_{1321} & D_{1331} & D_{1341} \\ D_{1421} & D_{1431} & D_{1441} \end{bmatrix}$$

$$\approx \begin{bmatrix} 0 & 0 & 0 \\ 0 & \Gamma\langle\hat{\sigma}_{11}\rangle & 0 \\ 0 & 0 & \Gamma\langle\hat{\sigma}_{11}\rangle \end{bmatrix}. \tag{B4}$$

Unlike the normal-ordered noise terms, Eq. (B4) indicates that the anti-normal-ordered noise correlations in this double- $\Lambda$  system do not disappear even in the case of weak probe and signal fields. In Appendix C, we will show that the anti-normal-ordered noise terms lead to the dissipation of the incident light fields.

## APPENDIX C: COMMUTATION RELATION OF THE FIELD OPERATORS

The frequency-domain commutation relation of the creation and annihilation operators for the probe field can be expressed as

$$\left[\tilde{a}_p(z,\omega),\tilde{a}_p^{\dagger}(z,\omega')\right] = \frac{L}{2\pi c}\delta(\omega - \omega'). \tag{C1}$$

We use Eq. (10) in Sec. II to calculate the communication relation of the probe field propagating through the double- $\Lambda$  atomic medium as follows:

$$\begin{split} \langle \tilde{a}_{p,L}^{\dagger} \tilde{a}_{p,L} \rangle &= |A^*|^2 \langle \tilde{a}_{p,0}^{\dagger} \tilde{a}_{p,0} \rangle + |B^*|^2 \langle \tilde{a}_{s,0}^{\dagger} \tilde{a}_{s,0} \rangle \\ &+ \frac{L}{2\pi c} \sum_{jk} \sum_{j'k'} \int_0^L \mathcal{P}_{jk} D_{jk,k'j'} \mathcal{P}_{j'k'}^* dz, \quad \text{(C2)} \\ \langle \tilde{a}_{p,L} \tilde{a}_{p,L}^{\dagger} \rangle &= |A^*|^2 \langle \tilde{a}_{p,0} \tilde{a}_{p,0}^{\dagger} \rangle + |B^*|^2 \langle \tilde{a}_{s,0} \tilde{a}_{s,0}^{\dagger} \rangle \\ &+ \frac{L}{2\pi c} \sum_{jk} \sum_{j'k'} \int_0^L \mathcal{P}_{j'k'}^* D_{k'j',jk} \mathcal{P}_{jk} dz, \quad \text{(C3)} \end{split}$$

where  $\mathcal{P}_{jk} = e^{-M(L-z)}\zeta_{jk}^p$ . Substituting Eqs. (C2) and (C3) into Eq. (C1), and combining the results of Eqs. (B3) and (B4), the expectation value of the commutator

of the output probe field is derived as

$$\left\langle \left[ \tilde{a}_{p,L}, \tilde{a}_{p,L}^{\dagger} \right] \right\rangle = \frac{L}{2\pi c} \left( |A^*|^2 + |B^*|^2 \right) + \frac{L}{2\pi c} \int_0^L (\mathcal{P}_{31}^* D_{1331} \mathcal{P}_{31} + \mathcal{P}_{41}^* D_{1441} \mathcal{P}_{41}) dz.$$
(C4)

Based on Eqs. (C1) and (C4), we obtain

$$\int_{0}^{L} (\mathcal{P}_{31}^{*} D_{1331} \mathcal{P}_{31} + \mathcal{P}_{41}^{*} D_{1441} \mathcal{P}_{41}) dz$$
$$= 1 - |A^{*}|^{2} - |B^{*}|^{2}. \tag{C5}$$

The left-hand side of Eq. (C5) comes from the contribution of anti-normal-ordered noise correlations. This indicates that once the output probe field is dissipated, i.e.  $|A^*|^2 + |B^*|^2 < 1$ , it must be caused by the anti-normal-ordered noise correlations. However, for a double- $\Lambda$  medium with a sufficiently large OD,  $|A^*|^2 + |B^*|^2 \approx 1$ , that is, the contribution of anti-normal-ordered noise terms approaches to zero, indicating that the vacuum field reservoir is unable to disturb the lossless system through quantum fluctuations. The formula for the output signal field can also be obtained as follows:

$$\int_{0}^{L} (\mathcal{Q}_{31}^{*} D_{1331} \mathcal{P}_{31} + \mathcal{Q}_{41}^{*} D_{1441} \mathcal{P}_{41}) dz$$

$$= 1 - |C^{*}|^{2} - |D^{*}|^{2}, \qquad (C6)$$

where  $Q_{jk} = e^{-M(L-z)} \zeta_{jk}^s$ .

- C. K. Hong, Z. Y. Ou, and L. Mandel, "Measurement of subpicosecond time intervals between two photons by interference," Phys. Rev. Lett. 59, 2044 (1987).
- [2] R. Lopes, A. Imanaliev, A. Aspect, M. Cheneau, D. Boiron, and C. I. Westbrook, "Atomic Hong-Ou—Mandel experiment," Nature, 520, 66 (2015).
- [3] F. Bouchard, Alicia Sit, Y. Zhang, R. Fickler, F. M. Miatto, Y. Yao, F. Sciarrino, and E. Karimi, "Two-photon interference: the Hong—Ou—Mande effect," Rep. Prog. Phys. 84, 012402 (2020).
- [4] I. Afek, O. Ambar, and Y. Silberberg, "High-NOON states by mixing quantum and classical light," Science 328, 879 (2010).
- [5] M. C. Tichy, "Interference of identical particles from entanglement to boson-sampling," J. Phys. B 47, 103001 (2014).
- [6] M. Erhard, M. Malik, M. Krenn, and A. Zeilinger, "Experimental Greenberger-Horne-Zeilinger entanglement beyond qubits," Nat. Photonics 12, 759 (2018).
- [7] H. Wang et al., "Boson Sampling with 20 Input Photons and a 60-Mode Interferometer in a 10<sup>14</sup>-Dimensional Hilbert Space," Phys. Rev. Lett. 123, 250503 (2019).
- [8] A. N. Boto, P. Kok, D. S. Abrams, S. L. Braunstein, C. P. Williams, and J. P. Dowling, "Quantum Interferometric Optical Lithography: Exploiting Entanglement to Beat

- the Diffraction Limit," Phys. Rev. Lett. 85, 2733 (2000).
- [9] M. W. Mitchell, J. S. Lundeen, and A. M. Steinberg, "Super-resolving phase measurements with a multiphoton entangled state," Nature (London) 429, 161 (2004).
- [10] M. Müller, H. Vural, C. Schneider, A. Rastelli, O. G. Schmidt, S. Höfling, and P. Michler, "Quantum-Dot Single-Photon Sources for Entanglement Enhanced Interferometry," Phys. Rev. Lett. 118, 257402 (2017).
- [11] E. Polino, M. Valeri, N. Spagnolo, and F. Sciarrino, "Photonic quantum metrology," AVS Quantum Sci. 2, 024703 (2020).
- [12] S. Ramelow, L. Ratschbacher, A. Fedrizzi, N. K. Langford, and A. Zeilinger, "Discrete Tunable Color Entanglement," Phys. Rev. Lett. 103, 253601 (2009).
- [13] C. Joshi, A. Farsi, S. Clemmen, S. Ramelow, and A. L. Gaeta, "Frequency multiplexing for quasi-deterministic heralded single-photon sources," Nat. Commun. 9, 847 (2018).
- [14] M. Kues, C. Reimer, J. M. Lukens, W. J. Munro, A. M. Weiner, D. J. Moss, and Roberto Morandotti, "Quantum optical microcombs." Nat. Photonics 13, 170 (2019).
- [15] G. Maltese, M. I. Amanti, F. Appas, G. Sinni, A. Lemaître, P. Milman, F. Baboux and S. Ducci, "Generation and symmetry control of quantum frequency combs," npj Quantum Information 6, 13 (2020).

- [16] H.-P. Lo and H. Takesue, "Precise tuning of singlephoton frequency using an optical single sideband modulator," Optica 4, 919 (2017).
- [17] P. Imany, O. D. Odele, M. S. Alshaykh, H.-H. Lu, D. E. Leaird, and A. M. Weiner, "Frequency-domain Hong-Ou-Mandel interference with linear optics," Opt. Lett. 43 (12), 2760 (2018).
- [18] H.-H. Lu, J. M. Lukens, N. A. Peters, B. P. Williams, A. M. Weiner, and P. Lougovski, "Quantum interference and correlation control of frequency-bin qubits," Optica 5, 1455 (2018).
- [19] T. Kobayashi et al., "Frequency-domain Hong-Ou-Mandel interference," Nat. Photonics 10, 441 (2016).
- [20] Y. Chen, M. Fink, F. Steinlechner, J. P. Torres and R. Ursin, "Hong-Ou-Mandel interferometry on a biphoton beat note," npj Quantum Information 5, 43 (2019).
- [21] C. Joshi et al., "Frequency-Domain Quantum Interference with Correlated Photons from an Integrated Microresonator," Phys. Rev. Lett. 124, 143601 (2020).
- [22] A. K. Kashi and M. Kues, "Spectral Hong-Ou-Mandel Interference between Independently Generated Single Photons for Scalable Frequency-Domain Quantum Processing," Laser Photon. Rev. 15, 2000464 (2021).
- [23] J. S. Pelc, C. Langrock, Q. Zhang, and M. M. Fejer, "Influence of domain disorder on parametric noise in quasi-phase-matched quantum frequency converters," Opt. Lett. 35, 2804 (2010).
- [24] M. Fleischhauer, A. Imamoglu, and J. P. Marangos, "Electromagnetically induced transparency: Optics in coherent media," Rev. Mod. Phys. 77, 633 (2005).
- [25] C.-Y. Cheng, J.-J. Lee, Z.-Y. Liu, J.-S. Shiu, and Y.-F. Chen, "Quantum frequency conversion based on resonant four-wave mixing," Phys. Rev. A 103, 023711 (2021).
- [26] M. O. Scully and M. S. Zubairy, Quantum Optics (Cambridge University Press, Cambridge, England, 1997).
- [27] E. A. Korsunsky and D. V. Kosachiov, "Phase-dependent nonlinear optics with double- $\Lambda$  atoms," Phys. Rev. A **60**, 4996 (1999).
- [28] Y.-H. Chen, P.-J. Tsai, I. A. Yu, Y.-C. Chen, and Y.-F. Chen "Phase-dependent double-Λ electromagnetically induced transparency," arXiv:1409.4153.
- [29] M. Artoni and A. Zavatta, "Large Phase-by-Phase Modulations in Atomic Interfaces," Phys. Rev. Lett. 115, 113005 (2015).
- [30] Z.-Y. Liu, Y.-H. Chen, Y.-C. Chen, H.-Y. Lo, P.-J. Tsai, I. A. Yu, Y.-C. Chen, and Y.-F. Chen, "Large Cross-Phase Modulations at the Few-Photon Level," Phys. Rev. Lett. 117, 203601 (2016).
- [31] S. Sagona-Stophel, R. Shahrokhshahi, B. Jordaan, M. Namazi, and E. Figueroa, "Conditional  $\pi$ -Phase Shift of Single-Photon-Level Pulses at Room Temperature," Phys. Rev. Lett. **125**, 243601 (2020).
- [32] B. Kim and H. Kang, "Cross-phase modulation between pulse matched lights in optical loop system," Opt. Commun. 508, 127753 (2022).
- [33] M. Fleischhauer and M. D. Lukin, "Quantum memory for photons: Dark-state polaritons," Phys. Rev. A 65, 022314 (2002).
- [34] P. Kolchin, "Electromagnetically-induced-transparencybased paired photon generation," Phys. Rev. A 75, 033814, (2007).
- [35] H. Hsu, C.-Y. Cheng, J.-S. Shiu, L.-C. Chen, and Y.-F. Chen, "Quantum fidelity of electromagnetically induced transparency: the full quantum theory," Opt. Express

- **30**, 2097 (2022).
- [36] N. Lauk, C. O'Brien, and M. Fleischhauer, "Fidelity of photon propagation in electromagnetically induced transparency in the presence of four-wave mixing," Phys. Rev. A 88, 013823 (2013).
- [37] K.-F. Chang, T.-P. Wang, C.-Y Chen, Y.-H. Chen, Y.-S. Wang, Y.-F. Chen, Y.-C. Chen, and I. A. Yu, "Low-loss high-fidelity frequency beam splitter with tunable split ratio based on electromagnetically induced transparency," Phys. Rev. Research 3, 013096 (2021).
- [38] M.-J. Lee, J. Ruseckas, C.-Y. Lee, V. Kudriašov, K.-F. Chang, H.-W. Cho, G. Juzeliānas, and I. A. Yu "Experimental demonstration of spinor slow light," Nat. Commun. 5, 5542 (2014).
- [39] M. A. Nielsen and I. L. Chuang, Quantum Computation and Quantum Information (Cambridge University Press, Cambridge, 2000).
- [40] C.-K. Chiu, Y.-H. Chen, Y.-C. Chen, I. A. Yu, Y.-C. Chen, and Y.-F. Chen, "Low-light-level four-wave mixing by quantum interference," Phys. Rev. A 89, 023839 (2014).
- [41] C.-Y. Lee, B.-H. Wu, G. Wang, Y.-F. Chen, Y.-C. Chen, and I. A. Yu, "High conversion efficiency in resonant fourwave mixing processes," Optics Express 24, 1008 (2016).
- [42] Z.-Y. Liu, J.-T. Xiao, J.-K. Lin, J.-J. Wu, J.-Y. Juo, C.-Y. Cheng and Y.-F. Chen, "High-efficiency backward four-wave mixing by quantum interference," Sci. Rep. 7, 15796, (2017).
- [43] J.-Y. Juo, J.-K. Lin, C.-Y. Cheng, Z.-Y. Liu, I. A. Yu, and Y.-F. Chen, "Demonstration of spatial-lightmodulation-based four-wave mixing in cold atoms," Phys. Rev. A 97, 053815 (2018).
- [44] C.-Y. Cheng et al., "Efficient frequency conversion based on resonant four-wave mixing," Opt. Lett. 46, 681 (2021).
- [45] S. Slussarenko, M. M. Weston, H. M. Chrzanowski, L. K. Shalm, V. B. Verma, S. W. Nam, and G. J. Pryde, "Unconditional violation of the shot-noise limit in photonic quantum metrology," Nat. Photonics 11, 700 (2017).
- [46] F. Blatt, T. Halfmann, and T. Peters, "One-dimensional ultracold medium of extreme optical depth," Opt. Lett. 39, 446 (2014).
- [47] Y.-F. Hsiao, H.-S. Chen, P.-J. Tsai, and Y.-C. Chen, "Cold atomic media with ultrahigh optical depths," Phys. Rev. A 90, 055401 (2014).
- [48] K. T. Kaczmarek et al., "Ultrahigh and persistent optical depths of cesium in Kagomé-type hollow-core photonic crystal fibers," Opt. Lett. 40, 5582 (2015).
- [49] M. Saeedi, R. Wille and Rolf Drechsler, "Synthesis of Quantum Circuits for Linear Nearest Neighbor Architectures," Quantum Inf. Process 10, 355 (2011).
- [50] A. G. Fowler, M. Mariantoni, J. M. Martinis, and A. N. Cleland, "Surface codes: Towards practical large-scale quantum computation," Phys. Rev. A 86, 032324 (2012).
- [51] M. Fleischhauer and M. D. Lukin, "Dark-state polaritons in electromagnetically induced transparency," Phys. Rev. Lett. 84, 5094 (2000).
- [52] A. I. Lvovsky, B. C. Sanders, and W. Tittel, "Optical quantum memory," Nat. Photonics 3, 706 (2009).
- [53] Y.-F. Hsiao et al., "Highly Efficient Coherent Optical Memory Based on Electromagnetically Induced Transparency," Phys. Rev. Lett. 120, 183602 (2018).
- [54] P. Vernaz-Gris, K. Huang, M. Cao, A. S. Sheremet, and J. Laurat, "Highly-efficient quantum memory for polar-

- ization qubits in a spatially-multiplexed cold atomic ensemble," Nat. Commun. 9, 363 (2018).
- [55] Y. Wang et al., "Efficient quantum memory for singlephoton polarization qubits," Nat. Photonics 13, 346 (2019).
- [56] N. Jiang, Y.-F. Pu, W. Chang, C. Li, S. Zhang and L.-M. Duan, "Experimental realization of 105-qubit random access quantum memory," npj Quantum Information 5, 28 (2019).
- [57] H.-J. Briegel, W. Dür, J. I. Cirac, and P. Zoller, "Quantum Repeaters: The Role of Imperfect Local Operations in Quantum Communication," Phys. Rev. Lett. 81, 5932 (1998).
- [58] L.-M. Duan, M. D. Lukin, J. I. Cirac, and P. Zoller, "Long-distance quantum communication with atomic ensembles and linear optics," Nature 414, 413 (2001).
- [59] Z.-S. Yuan, Y.-A. Chen, B. Zhao, S. Chen, J. Schmied-mayer, and J.-W. Pan, "Experimental demonstration of a BDCZ quantum repeater node," Nature 454, 1098 (2008).
- [60] K. Hammerer, A. S. Sørensen, and E. S. Polzik, "Quantum interface between light and atomic ensembles," Rev. Mod. Phys. 82, 1041 (2010).
- [61] N. Sangouard, C. Simon, H. de Riedmatten, and N. Gisin, "Quantum repeaters based on atomic ensembles

- and linear optics," Rev. Mod. Phys. 83, 33 (2011).
- [62] S. Langenfeld, O. Morin, M. Körber and G. Rempe, "A network-ready random-access qubits memory," npj Quantum Information 6, 86 (2020).
- [63] X. Liu et al., "Heralded entanglement distribution between two absorptive quantum memories," Nature 594, 41 (2021).
- [64] H. J. Kimble, "The quantum internet," Nature 453, 1023 (2008).
- [65] F. Mei, M. Feng, Y.-F. Yu, and Z.-M. Zhang, "Scalable quantum information processing with atomic ensembles and flying photons," Phys. Rev. A 80, 042319 (2009).
- [66] S. D. Barrett, P. P. Rohde, and T. M. Stace, "Scalable quantum computing with atomic ensembles," New J. Phys. 12, 093032 (2010).
- [67] C. Simon, "Towards a global quantum network," Nat. Photonics 11, 678 (2017).
- [68] H. Li et al., "Multipartite entanglement of billions of motional atoms heralded by single photon," npj Quantum Information 7, 146 (2021).
- [69] J. C. Garrison and R. Y. Chiao, Quantum Optics (Oxford Graduate Texts, 2014).